ACS OMEGA

Open Access

http://pubs.acs.org/journal/acsodf

Article

Exploring the Potential Fungicidal Applications of a Cu(II) Complex with Schiff Base and Carboxylates against *Fusarium equisetum*

Arun Kuila, Ribhu Maity, Prasun Acharya, Tuhin Sarkar, Ankika Bhakat, Paula Brandao, Satyajit Pattanayak, Tithi Maity, Sudipta Dalai,* Keka Sarkar,* and Bidhan Chandra Samanta*

Cite This: *ACS Omega* 2024, 9, 48273−48284

Read Online

ACCESS | Metrics & More | Article Recommendations | Supporting Information

ABSTRACT: Given the critical need to preserve agricultural sustainability, there is an urgent call to address fungal infections. Our study presents a promising approach by focusing on SIX (Secreted in Xylem) proteins as a pivotal target for the development of innovative fungicidal strategies. Within the sphere of this study, we meticulously scrutinize the antifungal efficacy of our synthesized Cu(II) complex formulated as $[Cu(L1)_2(L2)]^+(ClO_4)^-$, where L1 represents (*E*)-cyclohexyl−*N*(pyridine-2-xlmethylene) methanamine and L2H denotes cinnamic acid, compared against a commercially available fungicide comprising 4% hexaconazole and 68% zineb. Employing in silico methodologies, we undertake a comparative analysis targeting SIX proteins to discern the potency of our compound. The X-ray diffraction, ^{1}H NMR, and FTIR spectroscopic techniques were utilized to elucidate the structure of the complex methodically. The lipophilicity test of the complex signifies its potential lipophilic nature and prompted further investigation into the complex's interaction with DNA (DNA) and bovine serum albumin (BSA). The binding constant values suggested a notable interaction between the complex and both DNA and BSA. The antifungal test reveal that our complex emerges as a potent contender in the battle against Fusarium equisetum (F.E.), exhibiting a commendable efficacy that positions it as a viable substitute for the incumbent commercial fungicide. This discovery predicts well the prospect of bolstering agricultural resilience and safeguarding global food security in the face of pervasive fungal threats.

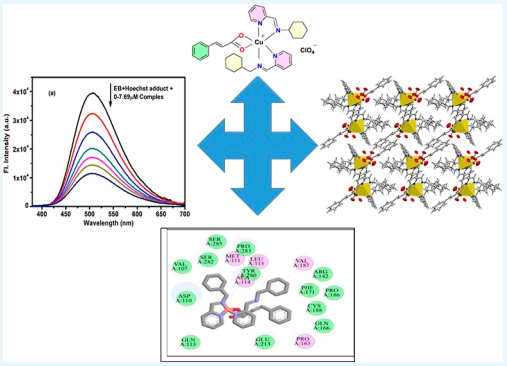

1. INTRODUCTION

The quest for novel metal-based antimicrobial agents represents a frontier in medicinal chemistry with researchers actively engaged in the design and synthesis of compounds with enhanced efficacy, selectivity, and safety profiles. Synthetic chemists are increasingly drawn to exploring new metal complexes as candidates for bioactive compounds. These complexes offer structures and properties that can be tailored to target specific microbial pathogens. Moreover, the versatility of metal complexes allows for the development of innovative therapeutic approaches to address the challenges posed by drug resistance and the complexity of infectious diseases.[1,2] Despite the availability of various antibacterial and antifungal compounds, microorganisms continue to develop resistance against them. Consequently, discovery of new class of drugs with enhanced activity and selectivity is needed to combat multidrug-resistant infections effectively.[3,4]

In this context, Schiff bases and their metal complexes have garnered attention as promising candidates for drug development.[5−7] Schiff bases are versatile organic compounds derived from the condensation reaction between a primary amine and a carbonyl compound demonstrating a variety of biological activities such as antibacterial, anticancer, and antifungal activities. Moreover, when Schiff bases are coordinated with metal ions, they often display enhanced pharmacological properties, such as increased stability and improved bioavailability. The potential of Schiff bases and their metal complexes in addressing drug resistance stems from their ability to interact with microbial targets through diverse mechanisms. These compounds can disrupt essential biological processes in microorganisms, such as cell wall synthesis, protein synthesis, and DNA replication, thereby exerting potent antimicrobial effects. These compounds offer promising avenues for discovering next-generation antimicrobial agents capable of overcoming the challenges of multidrug resistance.

Moreover, in recent years, researchers have found a burgeoning interest in investigating the intricate dynamics governing the interactions between metal complexes and biomolecules, particularly DNA and proteins.[8−17] These endeavors are driven by a quest for a comprehensive understanding of crucial processes such as drug transportation

Received: June 22, 2024
Revised: October 19, 2024
Accepted: November 13, 2024
Published: November 22, 2024

Scheme 1. Synthetic Route for the Ligand and the Complex

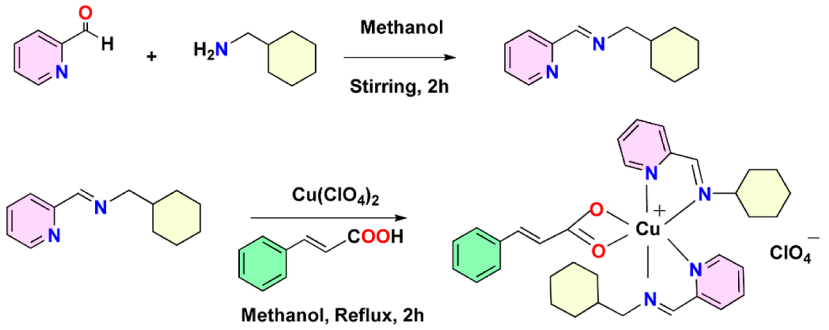

and metabolism, which catalyze the development of novel metallo-pharmaceuticals. The exploration of organometallic complexes' interaction with biomolecules, notably DNA and bovine serum albumin (BSA), serves as a cornerstone for unravelling the intricate mechanisms underlying their binding phenomena. Given the pivotal role DNA plays in the context of numerous anticancer and antifungal therapies, elucidating the binding interactions between metal complexes and DNA emerges as a paramount endeavor for developing prospective DNA-targeting antiproliferative therapeutic agents.

Besides, in the pursuit of elucidating the intricacies of binding mechanisms, BSA has emerged as a favored model in recent decades for its striking structural similarity with human serum albumin (HSA).[18,19] This structural similarity allows for insightful extrapolation of findings from studies utilizing BSA to human physiology, thus enhancing the translational potential of such research efforts.

In parallel, the significance of antioxidants in combating the deleterious effects of free radicals cannot be overstated. Free radicals, notorious for their involvement in numerous degenerative disorders that include carcinogenesis, cardiac disorders, mutagenesis, and aging, pose a significant threat to biological systems. Therefore, assessing antioxidant capacity, particularly the free-radical scavenging activity, of compounds earmarked for use as antitumor drugs assumes paramount importance.[20,21] Among the plethora of methods available for evaluating antioxidant potential, the 2,2-diphenyl-1-picrylhydrazyl (DPPH) free-radical scavenging technique stands out for its simplicity, rapidity, cost-effectiveness, and widespread applicability.[22] This method offers a reliable means of gauging the ability of compounds to neutralize free radicals, thereby providing crucial insights into their potential therapeutic efficacy. In light of these considerations, our current study endeavors to shed light on the antioxidant capacity of the investigated complexes using the DPPH method. Furthermore, we aim to unravel the intricate binding interactions between these complexes and biomolecules, such as DNA and BSA, employing various spectroscopic techniques. By elucidating these fundamental aspects, our research endeavors to contribute to the broader understanding of metal complex-biomolecule interactions and pave the way for developing innovative therapeutic interventions of improved efficiency and selectivity.

The current work aims to explore the synthesis and characterization of a copper complex from a Schiff base ligand L1 derived from pyridine 2-aldehyde and amino methyl cyclohexane and a coligand L2. The complex's in vitro antifungal activities against F.E. have been investigated through combined experimental and in silico approaches. F.E. stands as a formidable adversary in the realm of plant pathogens, demonstrating a remarkable ability to thrive across diverse environments from the lush tropics to the temperate climes. Its deleterious impact is felt keenly through symptoms such as vascular blockage, leaf yellowing, and, in severe instances, the demise of afflicted plants. This pathogen initiates its insidious assault by exploiting wounds in the plant's integument, infiltrating the root cortex, and fomenting disease onset. Initially assuming the guise of biotrophic fungi, these insidious invaders transition to a necrotrophic stage, unleashing a barrage of toxins and cellulolytic enzymes to fortify their foothold and plunder the host's vital nutrients.

Among cereals like wheat, oats, barley, and maize, Fusarium reigns as a chief nemesis, casting its shadow with the production of mycotoxins.[23] Its detrimental reach extends further into the realm of tropical fruit crops, such as banana and pineapple, as well as lentils, tomatoes, and peas, where it exacts a heavy toll, precipitating up to a staggering 50% reduction in crop yields.[24,25] The moment of infiltration marks the inception of a sinister dialogue between the pathogen and host, facilitated by the channel of the xylem sap. Within this clandestine exchange, a set of proteins known as SIX (Secreted in Xylem) assumes the mantle of pathogenicity, orchestrating the march of disease.[26−28] So, in this current study, we methodically examine the antifungal effectiveness of our synthesized complex, contrasting it with a commercially available fungicide containing 4% hexaconazole and 68% zineb. Using in silico methods, we conducted a comparative analysis focusing on SIX proteins to assess the efficacy of our compound. Hexaconazole, a famous chemical fungicide, is applied by Indian farmers to fight the aforesaid pathogens. We observed that compared to hexaconazole, the present complex demonstrated noteworthy antifungal activity. So, the results demonstrated the complex's antifungal ability against F.E. and highlighted its promise as a novel candidate for combating fungal pathogens in agricultural and pharmaceutical contexts. This is the motivation and novelty of the current work.

2. MATERIALS AND METHODS

2.1. Materials. The required materials for the current experiments were used without undergoing additional purification steps. Pyridine-2-aldehyde, amino methyl cyclohexane, cinnamic acid, methanol, copper(II) perchlorate hexahydrate [$Cu(ClO_4)_2{\cdot}6H_2O$], DPPH, and Hoechst have been purchased from Merck. Serum albumin and CT-DNA were procured from Sigma-Aldrich Chemicals (USA). The phosphate buffer of 7.4 (10 mM) was used for the solution preparation.

https://doi.org/10.1021/acsomega.4c05824
ACS Omega 2024, 9, 48273−48284

2.2. Preparation of the Ligand L1. The synthesis process involved stirring a mixture comprising 1 mmol each of pyridine-2-aldehyde and amino methyl cyclohexane in methanol for a duration of 2 h (Scheme 1). During this period, the reaction mixture underwent a transformation, resulting in the formation of a yellow-colored solution. Subsequently, this solution was directly utilized to synthesize the complex.

Yield: 95%. Molecular formula $C_{13}H_{18}N_2$, FTIR spectral data (KBr, cm^{-1}; s = strong, vs = very strong, br = broad, m = medium): 3434 (br), 2926 (m), 1628 (m), 1261 (m). Absorption maximum in MeOH [λ_{max}, nm]: 343. m/z value in the mass spectrum: Projected for [$C_{13}H_{18}N_2$] 202.15, observed with H^+ ion 203.15.

2.3. Complex Synthesis. The complex was synthesized through a refluxing process involving a mixture comprising copper(II) perchlorate hexahydrate (0.5 mmol), L1, and cinnamic acid (L2; 1 mmol) in methanol. This refluxing step lasted approximately 2 h. A distinct green-colored solution was obtained on completion of the reaction. Then, a slow vaporization technique was employed for the crystallization. After several days, green type single crystals suitable for X-ray diffraction to elucidate the crystal structure were obtained (Scheme 1).

Yield: 80%. Molecular formula $C_{35}H_{43}ClCuN_4O_6$, FTIR spectral data (KBr, cm^{-1}; s = strong, vs = very strong, br = broad, m = medium): 3436 (br), 2926 (m), 2851 (m), 1640 (m), 1377 (s), 1103 (s). UV absorption in MeOH [λ_{max}, nm]: 665. 1H NMR (DMSO−D6, 500 MHz): 1.08 (cyclohexane protons), 1.63 (2H, d, − N−CH_2), 2.46 (DMSO−D6), 2.93 (H_2O), 7.30−7.61 (Ar−protons), 4.51 (1H, s, N═CH).

2.4. Characterizations and Testing. The UV−Vis spectrophotometer 2202 (Systronic, India) and Shimadzu IR Affinity −1S spectrometer were employed for UV and FT-IR studies, respectively. For mass analysis, a Bruker Daltonics micrOTOF-Q mass spectrometer was used. NMR studies were carried out in a JEOL JNM-ECS400 spectrometer at ambient temperatures with $CHCl_3$ (δ = 7.26 ppm) and DMSO-d_6 (δ = 2.50 ppm) as references. Scanning electron microscopy (ZEISS EVO LS 10) was employed for microscopic imaging.

2.5. X-ray Diffraction Studies. To collect the X-ray diffraction data, RIGAKU XtaLAB Synergy-i furnished with a Mo Kα (λ = 0.71073 Å) PhotonJet-i microsource, a HyPix3000 detector well-ordered by the CrysAlisPro software (Y. Oxford Diffraction Ltd., England, 2022, CrysAlis PRO, Rigaku V1.171.142.173a) and fortified with an Oxford Cryosystems Series 800 cryostream was employed. Diffraction data were analyzed with CrysAlisPro software, and absorption effects were addressed through multiscan correction utilizing spherical harmonics, as implemented in the SCALE3 ABSPACK scaling algorithm. The structures were determined using direct methods with SHELXT 2014/5 and refined through weighted full-matrix least-squares on F^2 using SHELXL2018/3.[29] Anisotropic thermal parameters were applied to all non-hydrogen atoms during refinement. One oxygen from the perchlorate anion is disordered over two positions (occupancies refined as x and $1-x$). Mercury software was used to draw molecular diagrams.[30] Table 1 shows the crystal data and key refinement details. The CCDC number for the complex gained from the CCDC Centre[31] is 2347314.

2.6. Lipophilicity Test. The lipophilicity of the complex was assessed using the Flask-shaking technique measuring partition coefficient among n-octanol and water (Log $P_{o/w}$).[32] To execute the process, the complex (0.001 g) was mixed with 10 mL of solution of octanol and water (1:1 V/V) at 298 K. By applying the Beer−Lambert law to determine the concentration of the complex in both phases, the lipophilicity value has been then calculated by eq 1.

$$\text{Log } P_{o/w} = \log([\text{complex}] \text{ in octanol phase}/[\text{complex}] \text{ in water phase}) \quad (1)$$

Table 1. Key Refinement Details and Crystal Data for the Complex [$Cu(L1)_2L2$]

empirical formula	$C_{35}H_{43}ClCuN_4O_6$
M_w	714.72
crystal system	triclinic
space group	$P\bar{1}$
a/[Å]	11.95050(15)
b/[Å]	12.07453(13)
c/[Å]	13.71614(17)
α/[°]	79.5360(10)
β/[°]	76.0197(11)
γ/[°]	68.4106(11)
V [Å^3]	1776.38(4)
Z	2
D_c [Mg m^{-3}]	1.336
μ/[mm^{-1}]	0.739
F(000)	750
crystal size [mm^3]	0.22 × 0.14 × 0.04
θ range for data collection (°)	2.121−27.492
index ranges	$-15 \le h \le 15$, $-15 \le k \le 15$, $-17 \le l \le 17$
reflections collected	52,952
unique reflections, [R_{int}]	7700[0.0268]
final R indices	
R_1, wR_2 [$I > 2\sigma I$]	0.0459, 0.12012 [6706]
R_1, wR_2 (all data)	0.0534, 0.1249
data/restraints/parameters	7700/6/441
goodness-of-fit on F^2	1.074

2.7. Antioxidant Studies by the DPPH Method. Antioxidant studies were conducted by using the DPPH method. This assay involves DPPH free radicals scavenging (structure shown below) for evaluating the potential antioxidant properties for the complex, following a standard protocol.[33] To prepare the working solution, first of all the complex was mixed with a solution of 1:1 DMSO and H_2O. A solution of 50 μM DPPH in methanol was prepared separately. Various concentrations (ranging from 0 to 1454 μM) of the complex solution in DMSO (0 to 3 mL) were mixed to 5 mL of the DPPH solution. The solution was shaken vigorously and then allowed to incubate in the dark at room temperature for 30 min. The decrease in DPPH absorbance at 517 nm was monitored for both the complex and ascorbic acid (AA), which served as the standard. Additionally, color changes in the pure DPPH solution were noticed on regular addition of AA (ranging from 0 to 46 μM) and the complex (ranging from 0 to 1454 μM). The DPPH scavenging activity was determined using Formula 2

$$\text{scavenging activity (\%)} = [(A_0 - A_1)/A_0] \times 100 \quad (2)$$

where A_0 represents the DPPH absorbance in the absence of an antioxidant, and A_1 represents the DPPH absorbance in the presence of the oxidant. The IC50 value, representing the

https://doi.org/10.1021/acsomega.4c05824
ACS Omega 2024, 9, 48273−48284

concentration at which 50% of the activity is achieved, was determined based on the percentage of activity.

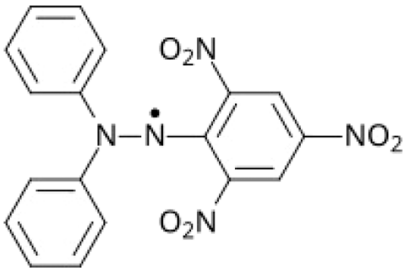

Structure of DPPH

2.8. Binding Interaction with DNA. Binding interactions with DNA were meticulously examined using an UV−vis spectrophotometer. The experimental procedure involved systematically adding varying concentrations of DNA (0 to 2.15 μM) to a certain complex concentration (870 μM), all in the presence of a reference buffer solution. Intrinsic binding constant (K_{ib}) has been determined from the Wolfe−Shimmer eq 3.

$$[\mathrm{DNA}] \times (\varepsilon_a - \varepsilon_f)^{-1} = [\mathrm{DNA}] \times (\varepsilon_b - \varepsilon_f)^{-1} + K_{ib}^{-1} \times (\varepsilon_b - \varepsilon_f)^{-1} \quad (3)$$

where ε_a signifies extinction coefficients of the complex, ε_f, signifies extinction coefficients of CT-DNA, and ε_b denotes extinction coefficients of the bound complex. The K_{ib} value was calculated from the ratio of slope to intercept of ([DNA]/(ε_a − ε_f)) vs [DNA] plot.

To explore deeper into the dynamics of this interaction, emission studies were conducted using a Shimadzu RF-6000 spectrofluorophotometer, covering a broad spectral range from 200 to 700 nm. This comprehensive analysis allowed for a thorough investigation into the behavior and effects of DNA on the complex, shedding light on its interaction mechanisms and properties across different wavelengths.

2.9. Interaction Study of the Complex with BSA. An in-depth investigation into the interaction of BSA was conducted using both absorption and emission spectroscopic methods. The study commenced with UV−vis spectroscopy, where alterations in the absorption spectra of the complex were meticulously observed at 665 nm. This observation was made while the concentrations of BSA were systematically increased, ranging from 0 to 0.314 μM.

In parallel, fluorescence spectroscopy was employed to scrutinize the interaction further. Specifically, changes in the fluorescence emission were recorded at 337 nm. This was achieved by incrementally increasing the concentrations of the complex from 0 to 70.76 μM.

These dual spectroscopic approaches enabled a comprehensive examination of the dynamic interplay between BSA and the studied complex. They provided valuable insights into the molecular-level mechanisms and characteristics of their interactions across different concentration ranges and spectral wavelengths.

2.10. Antifungal Test. *2.10.1. In Vitro Antifungal Assay.* The efficacy of the complex against F.E. was assessed using the agar cup assay,[34] an in vitro antifungal assay. In order to check the antifungal activity of the complex, the complex solution was first prepared at 5 mg/mL concentration in 20% DMSO. The antifungal impact of the complex was then compared with that of a commercial antifungal comprising 4% hexaconazole + 68% zineb (HexZ) considered as positive control and also with 20% DMSO taken as negative control against F.E. Since the sample had notable antifungal activity at 5 mg/mL, the complex concentration was lowered for determining the minimum inhibitory concentration (MIC) value of the complex against F.E. Four more distinct dilute solutions consisting of 2.5, 1.25, 0.625, and 0.312 mg/mL were made in 20% DMSO to assess the antifungal activity in comparison to the control, which was only 20% DMSO. A 100 μL spore suspension (1×10^5 spores/ml) prepared just now was obtained from F.E pathogen (10 day old). After that, the spore suspension was evenly distributed on a potato dextrose agar (PDA) plate. The agar plate was then punctured with 6 mm diameter wells using sterile cork borers. 100 μL of 5 unlike complex concentrations was supplemented into every well, while 100 μL of 20% DMSO was also accompanied into remaining well on the identical PDA plate as control. For 48 h, plates were incubated at 28 °C. The surrounding zone of inhibition of every well was determined in millimeters following the nurture period.

2.10.2. Light Microscopy. Mycelia of F.E. from a 10 day-old culture plate was moved to test tubes with 5 mL of PDB and cultured for 12 h at 28 °C with gentle shaking. The MIC value of the complex was applied to the test tubes, and disinfected water was accompanied by the crude controls. Following that, every test tube was shaken at 170 rpm for 48 h at 28 °C. Then, one loopful of mycelia from the treated and control test tube was taken on glass slides free from grease and a little drop of lactophenol cotton blue stain was applied. The samples were seen by using a Leica light microscope (Wetzlar, Germany) with a 60× objective.

2.10.3. Molecular Docking. In-silico molecular docking study is now vigorously used to determine the bond interaction between SIX proteins and our complex. In this study, the protein structures were obtained from Protein Data Base (SIX1-PDB ID: 7T69, SIX3-PDB ID: 50D4) and denoted as the receptor. The crystallographic structure of our complex was transformed into.pdb format using Open Babel GUI. All the 3D structures were taken into Chimera (version-1.17.3) and protonated processed, and a grid box was setup for docking.[35] The molecules were docked via an inbuilt AutoDock vina manual, and the binding affinity was noted. After the docking, the receptor−ligand complex was further visualized in Discovery Studio Visualizer to find the binding pattern.[36]

3. DISCUSSION OF THE OBTAINED RESULTS

3.1. Synthetic and Spectroscopic Analyses for L1 and the Complex. Synthetic procedure of Schiff base L1 ligand involved stirring a mixture containing 1 mmol each of pyridine-2-aldehyde and amino methyl cyclohexane in methanol for a duration of 2 h. Subsequent to this, L1 was meticulously characterized utilizing absorption, FT-IR, and mass spectroscopic techniques.

The absorption spectrum of L1 (refer to Figure S1a, Supporting Information) exhibited absorption maximum at λ_{max} 343 nm. This peak signifies the wavelength at which the ligand predominantly absorbs light, indicating the presence of a conjugated system within the molecule. In the FTIR spectrum (refer to Figure S1b, Supporting Information), a notable peak appeared at 1628 cm^{-1}, corresponding to the imine (C═N) moiety confirming explicitly the development of the Schiff base. Furthermore, the peak corresponding to the normal region of the aldehyde group of pyridine-2-aldehyde is absent

https://doi.org/10.1021/acsomega.4c05824
ACS Omega 2024, 9, 48273−48284

suggesting its complete conversion during the Schiff base formation process. The aldehyde group has effectively undergone a transformation into the imine group upon reacting with amino methyl cyclohexane. In mass spectroscopic analysis (Figure S1c, Supporting Information), the strong peak achieved at 203.15 corresponded well to the m/z values of the projected structure with the H+ ion (m/z = 203.15), aligning consistently with the schematic structure of the ligand. Thus, the comprehensive spectroscopic analyses collectively validate the effective synthesis of ligand L1.

The synthesis of the complex was achieved through a refluxing process, wherein a mixture comprising $[Cu(ClO_4)_2 \cdot 6H_2O]$ (0.5 mmol), L1, and cinnamic acid (L2; 1 mmol) in methanol underwent a reaction. Comprehensive characterization of the resulting complex was conducted by employing various spectroscopic techniques, including absorption, FT-IR, and ^{1}H NMR spectroscopy.

In the absorption spectrum (refer to Figure S5, Supporting Information), a distinct peak was observed at a wavelength (λ_{max}) of 665 nm. This absorption peak serves as clear evidence of d−d transition due to the formation of pale blue color of the complex in methanol. Analysis of the FT-IR spectrum of the complex (refer to Figure S2a, Supporting Information) revealed notable changes with respect to that of ligand L1. Specifically, the peak corresponding to imine shifted to a higher region at 1640 cm^{-1}, as opposed to the position observed for ligand L1 (1628 cm^{-1}). This spectral shift suggests the active involvement of the imine group in the coordination to the copper ion. Additionally, the ^{1}H NMR spectrum (Figure S2b, Supporting Information) supports all of the prominent proton peaks at corresponding regions, aligning consistently with the schematic structure of the complex.

3.2. Description of Crystal Structures. The complex's crystal structure was meticulously elucidated utilizing single-crystal X-ray diffraction, leading to its formulation as $[Cu(L1)_2(L2)]^+(ClO_4)^-$, where L1 represents (*E*)-cyclohexyl−*N*(pyridine-2-xlmethylene) methanamine and L2H denotes cinnamic acid. This compound crystallized within the triclinic $P\bar{1}$ space group. Within this structure, the single Cu^{2+} metal center displays a coordination number of six and exhibits a pronounced Jahn−Teller distortion. It coordinates with four nitrogen atoms from ligand 1 and two oxygen atoms belonging to the carboxylate group from ligand 2. This coordination geometry resembles a highly distorted octahedron, where the equatorial plane consists of one oxygen and three nitrogens. The bond lengths found within this structure vary within the range of 1.995(2)−2.060(2) Å for Cu−N bonds, and Cu−O1 measures 2.001(2) Å. The apical positions are occupied by the second oxygen [Cu−O_2 = 2.610(2) Å] and by a nitrogen N4 from the ethylimino group [Cu−N_4 = 2.217(2) Å], as detailed in Table S1 and Figure 1.

The bond distances of N2 and N4 from ethylimino to C15 and C28, respectively, are measured at 1.274(2) and 1.267(2) Å, confirming the double bond between N2 and C15 and between N4 and C28. The charge of the metal center (Cu^{2+}) is balanced by the presence of one perchlorate anion and cinnamic acid.

The crystal packing of the complex, as illustrated in Figure 2, is primarily stabilized by nonclassic hydrogen bonding interactions of the C···H−O type originating from both L1 and L2 ligands, as well as from the oxygens associated with the chloride anion. These interactions play a crucial role in determining the arrangement of molecules within the crystal lattice. A comprehensive analysis of these hydrogen bonding interactions is provided in Table S2.

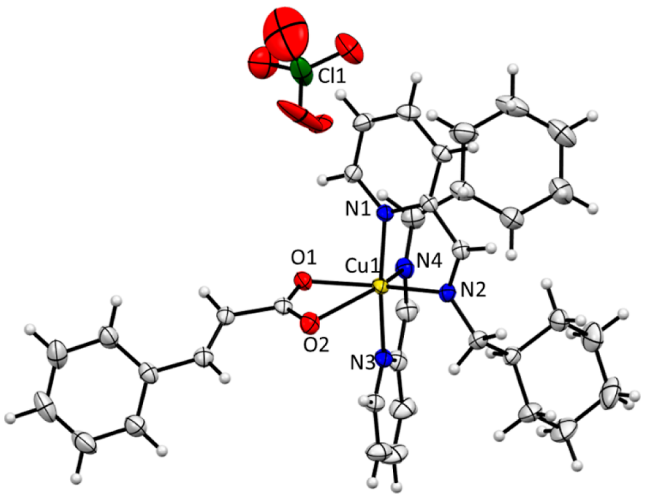

Figure 1. Ellipsoid view of $[Cu(L1)_2(L2)]^+(ClO_4)^-$ at 50% probability showing numbering of atom scheme.

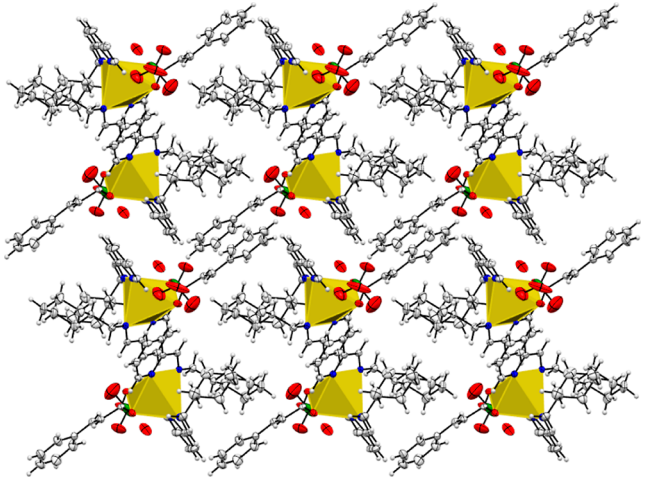

Figure 2. Crystal packing of $[Cu(L1)_2(L2)]^+(ClO_4)^-$ propagating along the '*a*' axis.

Furthermore, $\pi\cdots\pi$ intermolecular interactions occur between the pyridine rings of adjacent complex molecules. These interactions are supported by 3.645 Å interplanar distance and a shift of 1.232 distance (refer to Figure 3). These $\pi\cdots\pi$ interactions further contribute to the structural stability and organization of the crystal lattice.

Overall, the combined effects of $\pi\cdots\pi$ stacking and C···H−O interactions contribute significantly to the development of a three-dimensional assembly, as represented in Figure 2. This intricate network of intermolecular interactions governs the overall structural arrangement and stability of the complex within the crystal lattice.

3.3. Antioxidant and Lipophilicity Properties of the Complex. The study delved into the free-radical scavenging potential of the complex, assessed through IC50 values (representing 50% inhibition) using the DPPH oxidative assay method.[37] Figures S3a and S4a (Supporting Information) and Table 2 depict the results. Compared with ascorbic acid, employed as a standard, the IC50 value indicates the complex possesses a little free-radical scavenging capabilities. Additionally, evident color alterations in the DPPH violet solution upon

https://doi.org/10.1021/acsomega.4c05824
ACS Omega 2024, 9, 48273−48284

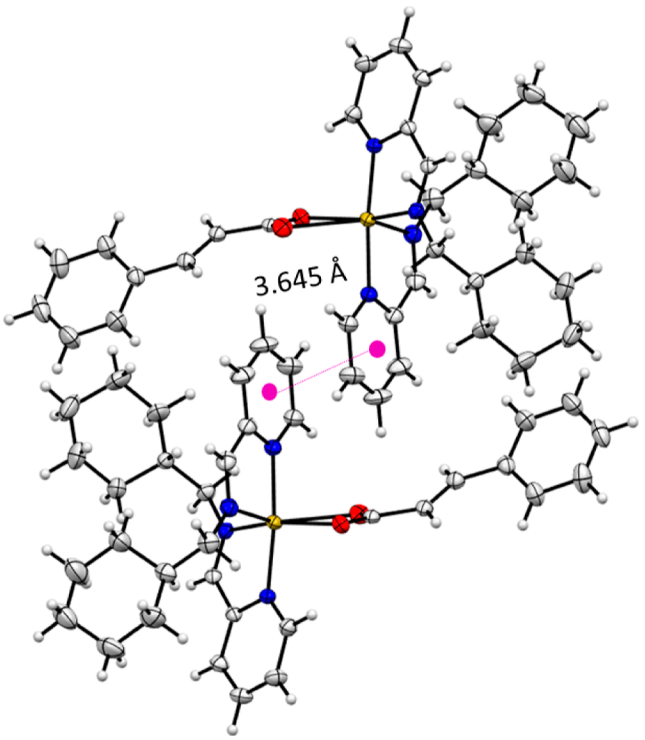

Figure 3. Intermolecular $\pi\cdots\pi$ stacking between two pyridine rings (N3, C23, C24, C25, C26, and C27 with $i = 1 - x, 1 - y, -z$).

Table 2. Values of IC50 Obtained in the DPPH Method

sample	IC50 value (μM)
$[Cu(L1)_2(L2)]^+(ClO_4)^-$	485
ascorbic acid	8

introducing the complex (Figure S3b and S4b, Supporting Information) corroborate these findings. These outcomes prompted further investigation into the complex's interaction with biomolecules such as DNA and BSA.

Before examining binding efficacy of the complex with DNA/BSA, complex stability in solution and its lipophilic character were assessed as outlined under the Methods section. The stability assessment study revealed consistent λ_{max} values of the complex solution over the span of 24 48 and 72 h (Figure S5, Supporting Information) with the same nature, representing extraordinary solution state stability of the complex.

The recorded log $P_{o/w}$ value (0.51) signifies the prospective lipophilic nature of the complex, akin to that of cisplatin, a renowned anticancer agent. Typically, cytotoxic agents exhibit log $P_{o/w}$ values ranging from −0.4 to 5.6, averaging at 2.52.[38] Hence, the observed log $P_{o/w}$ value, which is in between this range, indicates comparable lipophilic behaviors of the complex with the reported cytotoxic agents. This enhanced lipophilicity often facilitates better cell membrane penetration, thereby increasing drug accumulation within abnormal cells. This heightened accumulation frequently correlates with augmented cytotoxicity in vitro, allowing the drug to show its effects in a more efficient manner within the cellular milieu. This discovery holds promise and justifies further exploration of the complex's effectiveness and mechanisms of action both in vitro and in vivo methods.

3.4. DNA and BSA Binding Interaction Studies.

3.4.1. DNA Interaction Studies. The absorption and emission investigations were conducted to explore the binding affinity of a molecule with DNA. Absorption spectroscopy emerged as a pivotal tool in this investigation, offering insights into the spectral changes. Upon incremental addition of CT-DNA (ranging from 0 to 2.15 μM), alterations in the spectra were noted for a free complex concentration of 870 μM (as depicted in Figure 4a). Notably, an increase in absorption at 665 nm was observed as DNA concentration increased, indicative of the interaction between the complex and DNA's double helical structure. Intrinsic binding constant (K_{ib}) calculated from $[DNA]/(\varepsilon_a - \varepsilon_f)$ versus [DNA] plot (Figure 4b) with the help of Wolfe−Shimmer eq 3 having the value of 1.754×10^6 suggested a notable binding interaction between the complex and DNA.[39,40]

To determine whether the binding mode involves intercalation or groove, we conducted quenching studies with a standard intercalator ethidium bromide (EB).[41] EB exhibits no emission on its own, but when it is bound to DNA, it emits significantly at 630 nm. Upon regular addition of complex to EB-DNA adduct, no notable intensity quenching was observed (Figure 5a) at temperature 298 K, indicating that the complex is unable to displace EB from CT-DNA sequence. The quenching constant was derived from the Stern−Volmer eq 4

$$F_0/F = K_{SV}[Q] + 1 \quad (4)$$

where F and F_0 are the emission intensities in the presence and absence of complex, respectively, K_{SV} denotes quenching constant, and $[Q]$ represents complex concentration. By

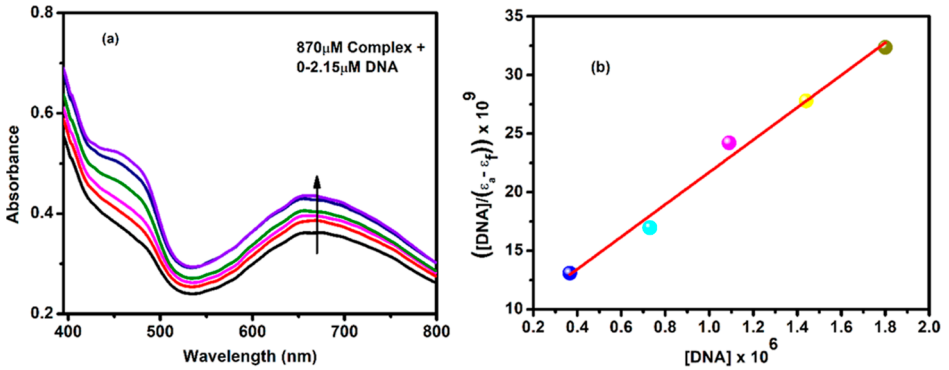

Figure 4. (a) UV−vis spectrum of complex (870 μM) in the presence of CT-DNA (0−2.15 μM) and (b) $[DNA]/(\varepsilon_a - \varepsilon_f)$ versus [DNA] plot for determining K_{ib}.

https://doi.org/10.1021/acsomega.4c05824
ACS Omega 2024, 9, 48273−48284

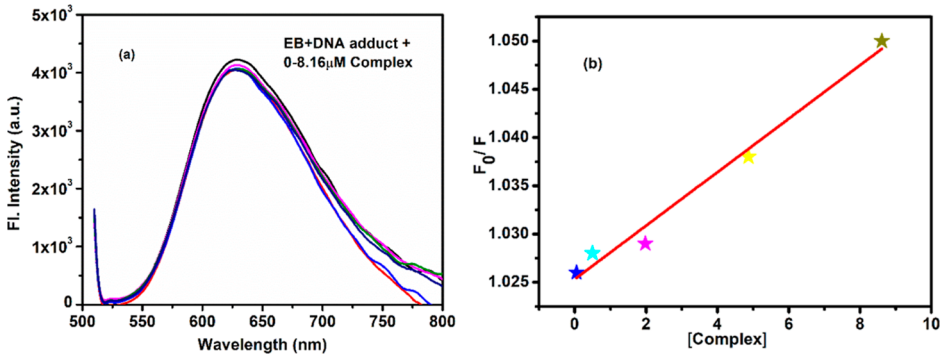

Figure 5. (a) Changes of emission intensity for CT-DNA—EB adduct with gradual addition of complex and (b) Stern−Volmer plot at 298 K.

analyzing the slope of the F_0/F versus [Q] plot, the K_{SV} value is calculated (Figure 5b) and the obtained value is shown in Table 3.

Table 3. Parameters Related to Binding Interaction of the Complex with DNA and BSA

binding system	K_{SV}	k_b value	n
EB-DNA + complex	2.77×10^4	3.58×10^4	0.098
EB-Hoechst + complex	3.40×10^5	2.42×10^6	1.19
BSA	3.82×10^4	6.90×10^4	0.832

Additionally, the number of binding sites (n) and binding constant (K_b) per DNA molecule were determined using the Scatchard eq 5

$$\log[(F_0 - F)/F] = \log K_b + n\log[\text{complex}] \quad (5)$$

The $\log[(F_0 - F)/F]$ versus log[complex] plot contributes a straight line (Figure S6a). The slope and intercept of this plot denote n and log K_b, respectively. All of the parameters as calculated are presented in Table 3, indicating not so efficiency of the complex in binding to CT-DNA in competitive experiments with EB.

In addition, we also conducted the binding interaction of a well-established DNA groove binder (Hoechst) with the complex. We monitored the variations in fluorescence intensity of the DNA-Hoechst adduct, centered around 506 nm, at 298 K, while gradually introducing the complex (Figure 6a). The quenching constant (K_{sv}), binding constant (K_b), and the number of binding sites (n) per DNA have been calculated from eqs 4 and 5 (Figures 6b and S6b). The values obtained for Hoechst displacement studies by the complex (as shown in Table 3) were much more significant than those observed in E.B. displacement studies at 298 K, indicating a groove binding mode for the complex with CT-DNA.

Furthermore, to provide additional confirmation regarding the binding mode, the stabilization of the DNA helix was assessed through helix melting experiments.[42] It is established that rise in helix melting temperature (T_m) of DNA (<5 °C) typically signifies groove mode of binding. In the present study, as depicted in Figure 7, the results indicate an increase in T_m of approximately 0.2 °C, supporting the conclusion of a groove mode of binding.

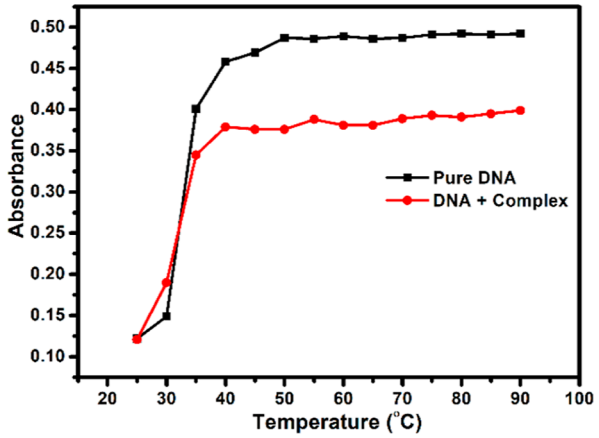

Figure 7. Melting profile of 30 μM untreated and treated DNA with a 20 μM complex.

3.4.2. Interaction of BSA with the Complex. Exploration of the biophysical binding dynamics between BSA and the complex was conducted using UV and fluorescence spectro-

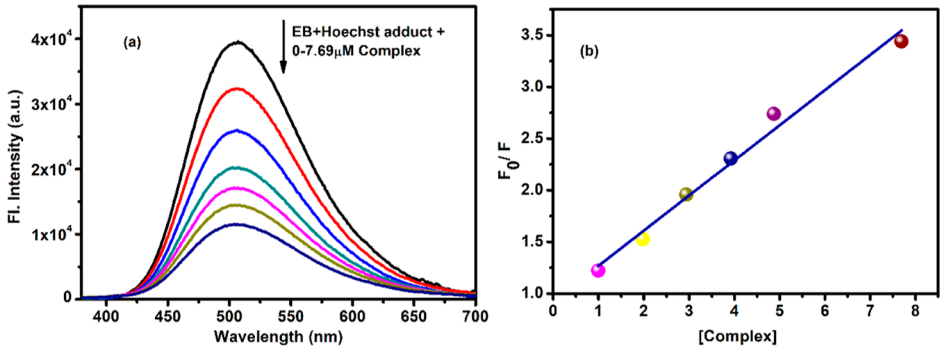

Figure 6. (a) Quenching spectra of DNA-Hoechst adduct and (b) Stern Volmer plot at 298 K.

https://doi.org/10.1021/acsomega.4c05824
ACS Omega 2024, 9, 48273−48284

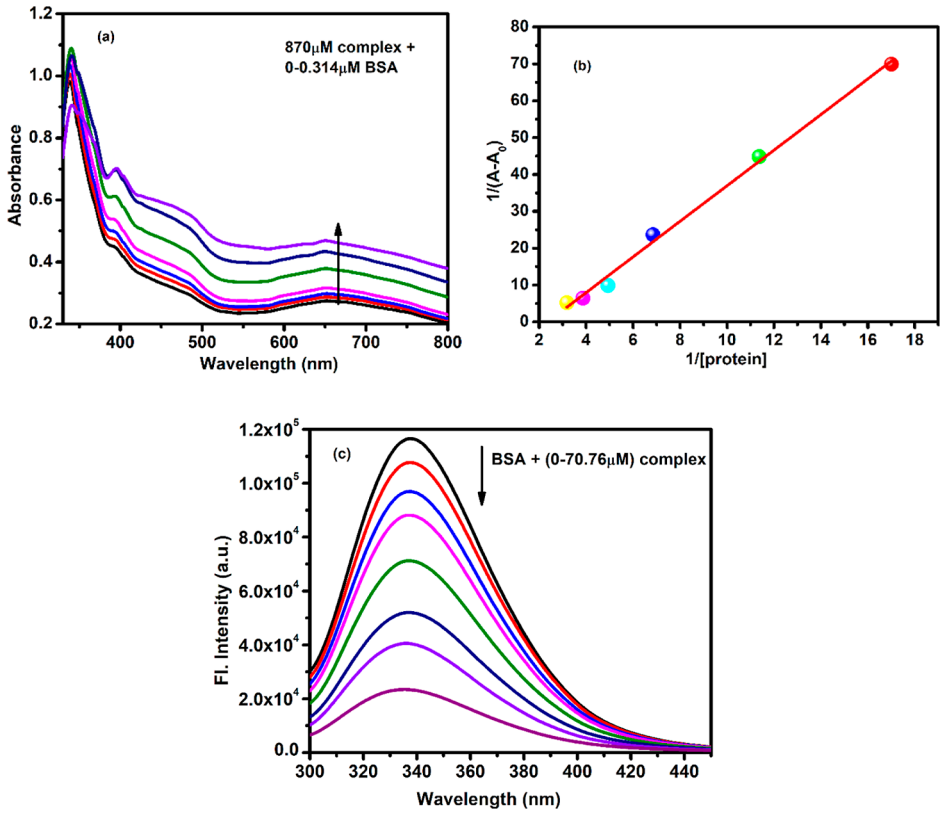

Figure 8. (a) Absorption spectrum of the complex (870 μM) in the presence of BSA (0 to 0.314 μM), (b) plot of $1/(A - A_0)$ versus 1/[protein], and (c) changes in fluorescence intensity of BSA at 337 nm with varied complex concentration from 0 to 70.76 μM.

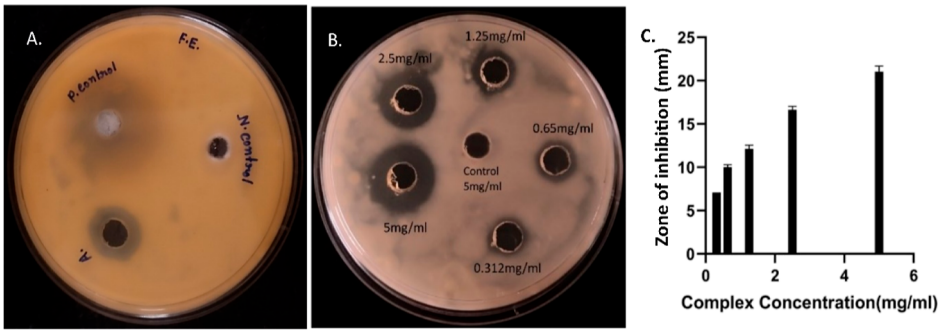

Figure 9. (A) Comparative analysis between the complex and a commercial antifungal compound, (B) zone of inhibition of the complex in a dose-dependent manner in comparison to control in the middle, and (C) graphical representation of ZOI at various concentrations (mg/mL).

scopic methods. Findings revealed a notable rise for a constant concentration of 870 μM complex absorption as the BSA concentration increased from 0 to 0.314 μM (Figure 8a), indicating a significant interaction between the two entities. The apparent association constant (K_{app}) was determined by utilizing eq 6.

$$1/(A_{obs} - A_0) = 1/(A_c - A_0) + 1/K_{app}(A_c - A_0)$$
$$[complex] \quad (6)$$

where A_{obs} denotes the observed absorbance of the solution, A_0 represents the absorbance of pure BSA, and A_c denotes the absorbance of the BSA-bound complex. The K_{app} value, derived from the plotted data (Figure 8b), stands at 8.71 × 10^4, aligning well with values reported for copper(II)−Schiff base complexes.[43,44]

Fluorescence investigations were conducted at 298 K, tracking changes in fluorescence intensity of BSA at 337 nm with the variance of complex concentrations from 0 to 70.76 μM. The results, as illustrated in Figure 8c, clearly indicate quenching with increasing complex concentration. Quenching constants (k_{sv}), binding constants (K_b), and the number of binding sites (n) per BSA were calculated by using eqs 4 and 5, respectively. The determined k_{sv}, K_b, and n values per BSA are presented in Table 3. Analysis, including the linear Stern−Volmer plot (Figure S7a) and the plot of $\log((F_0-F)/F)$ versus log[complex] (Figure S7b), suggests that the complex interacts with BSA via a single quenching mechanism.

We know that $K_{sv} = K_q\ \tau_0$, where K_{sv} is the Stern Volmer constant, K_q is the quenching constant, and τ_0 is the lifetime of fluorophore (here BSA).

Now for BSA, the τ_0 value is near 5 × 10^{-9} s and the K_{sv} for our study is in the order of 10^4 (Table 3). So, the quenching of

https://doi.org/10.1021/acsomega.4c05824
ACS Omega 2024, 9, 48273−48284

BSA by the complex (K_q) is in the order of 10^{13}, indicating static nature of quenching.[45] Static quenching physically indicates that the interaction between complex and BSA takes place in ground state.[33]

3.5. Results of Antifungal Test. *3.5.1. Fungal Growth Inhibition.* The antifungal efficacy of the complex was evaluated against F.E. using an agar cup assay. The findings of the study exposed inhibition of fungal growth in a dose-dependent manner, indicating the potency of the complex in controlling the proliferation of this pathogen. Across five different concentrations ranging from 5 mg/mL to 0.312 mg/mL, all exhibited a significant zone of inhibition surrounding the well against F.E. phytopathogens, with inhibition zones decreasing as concentrations decreased (Figure 9B). These findings were further depicted graphically in Figure 9C. Of particular note, the concentration of 0.312 mg/mL emerged as the MIC against F.E., underscoring the effectiveness of the complex in curbing fungal growth. A comparative analysis between the complex and a commercial antifungal compound, as illustrated in Figure 9A, confirmed the complex's ability to inhibit F.E. growth and suggested its potential as a viable alternative to existing market antifungal agents. In summary, the results demonstrated the complex's antifungal ability against F.E. and highlighted its promise as a novel candidate for combating fungal pathogens in agricultural and pharmaceutical contexts.

3.5.2. Effect of the Complex on the Mycelia Morphology of F.E. After 48 h of treatment with the complex at its MIC concentration, significant damage to the mycelia of F.E. was evident under light microscopy. Comparing the treated sample (Figure 10.B) with the control mycelia (Figure 10A) revealed

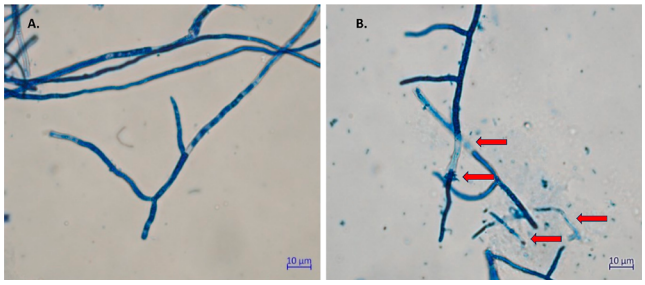

Figure 10. (A) Control mycelia of F.E. (scale bar = 10 μm, under 60× objective); (B) effect of complex against F.E. Disruption, loss of septation, and mycelial degradation detected on treated with MIC of complex by light microscopy post 48 h treatment (scale bar = 10 μm, under 60× objective).

marked differences in cellular integrity. The control mycelia exhibited proper septation and structural integrity, while the treated mycelia displayed extensive cell wall damage, evident morphological abnormalities, and signs of cellular leakage. This observation underscores the potent effect of the complex on disrupting the cell walls of F.E. mycelia. Such comprehensive damage points to a robust mechanism by which the complex targets and destabilizes fungal structures, ultimately impeding their growth and proliferation.

These outcomes offer appreciated insights into the mode of action of the complex against F.E., shedding light on its potential as a promising agent for combating fungal pathogens through targeted disruption of their cellular architecture.

3.5.3. Molecular Docking. The study delved into the examination and scoring of interactions involving SIX1, SIX3, and complex receptor−ligand interactions, yielding scores of −6.8 and −7.6, respectively (as illustrated in Figure 11). Specifically, SIX1 exhibited the formation of five pi−alkyl interactions along with 13 van der Waals contacts, while SIX3 showcased a range of interactions including two conventional hydrogen bonds, two pi−alkyl interactions, and eight van der Waals interactions.

These detailed molecular interactions provide critical insights into the mode of action of the complex in inhibiting SIX proteins, pivotal players in the pathogenicity of F.E. By elucidating the intricate network of receptor−ligand interactions, this analysis strengthens our understanding of how the complex effectively targets F.E.-mediated diseases at the molecular level. Such findings underscore the complex's potential as a therapeutic agent and lay the groundwork for developing more targeted and efficient strategies for combating fungal pathogens in agricultural and biomedical settings.

3.5.4. Discussion Comparing the Results of Our Previous Research with Current Results. In our previous research,[37] we explored the antifungal activity of a slightly distorted octahedral mononuclear Ni(II) complex resulting from a N, N, O donor Schiff base ligand against two fungal pathogens, viz., *Colletotrichum siamense* (AP1) and *Fusarium equisetum* (F.E.), and the results exposed momentous inhibitory effects of the complex on the growth of those fungal pathogens with MIC values 0.25 and 0.5 mM concentration, respectively. The comparative study between 0.1% hexaconazole and the synthesized Ni(II) complex revealed that the complex can be an alternative to the hexaconazole.

However in the current study, the antifungal efficiency of a Cu(II) complex was assessed against F.E. pathogen only, and the results exposed a dose-dependent inhibition of this fungal growth by the complex with a MIC value of 0.312 mg/mL, indicating the greater potency to some extent of the complex than the previous Ni(II) complex in controlling the growth of F.E. pathogen.

The antifungal impact of the present complex was also compared with that of a commercial antifungal comprising 4% hexaconazole +68% zineb (HexZ) as a positive control against F.E., indicating its potential as a viable alternative to existing market antifungal agents.

4. CONCLUSIONS

This study presents a multifaceted investigation encompassing the synthesis, characterization, crystal structure elucidation, and crystal packing of a Cu(II) complex derived from a N, N donor Schiff base ligand along with a coligand. Notably, the complex adopts a highly distorted octahedral geometry, with its equatorial plane comprising one oxygen and three nitrogens, while the apical positions are occupied by a second oxygen and a nitrogen N4 from an ethylimino group. Such structural intricacies lay the foundation for its diverse biological activities. Furthermore, the study delves into the biophysical insights regarding the complex's interactions with DNA and BSA. Through a range of spectroscopic techniques, robust binding interactions between the complex and both DNA and BSA are confirmed, indicating its potential as a therapeutic agent. Biological assays revealed significant inhibitory effects of the Cu(II) complex on the growth of the fungal pathogen F.E., with a MIC of 0.312 mg/mL. This underscores its potent antifungal activity and suggests its viability as an alternative to conventional antifungal agents in

https://doi.org/10.1021/acsomega.4c05824
ACS Omega 2024, 9, 48273−48284

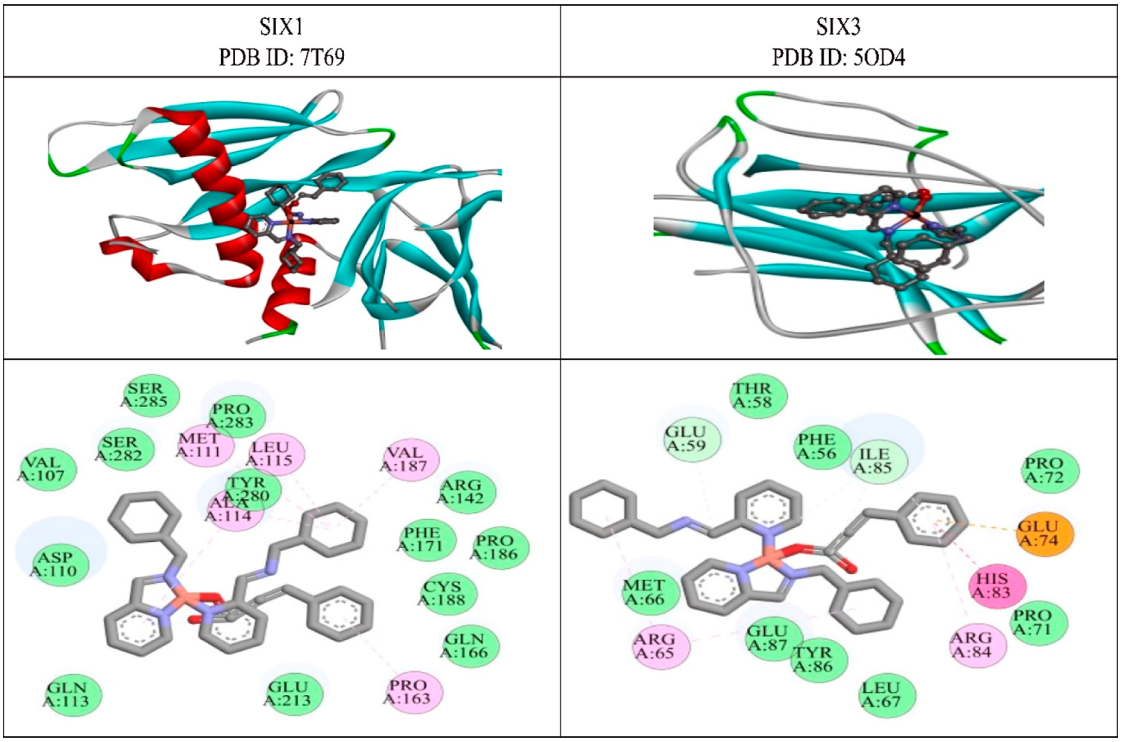

Figure 11. Molecular docking of SIX1 and SIX3 with the complex showing interactions between them.

agricultural contexts, where mitigating losses due to phytopathogens is crucial.

Combining theoretical predictions and experimental findings, this study provides compelling evidence of the Cu(II) complex's substantial antifungal activity against F.E. phytopathogens. Its potential application as a therapeutic fungicide in agricultural practices is thus underscored, highlighting the significance of this research in addressing agricultural challenges associated with fungal diseases.

■ ASSOCIATED CONTENT

Supporting Information

The Supporting Information is available free of charge at https://pubs.acs.org/doi/10.1021/acsomega.4c05824.

UV spectrum, FTIR spectrum, mass spectrum of the ligand L1; FTIR spectrum, 1HNMR spectrum of the complex; changes in absorbance of DPPH with gradual addition of ascorbic acid; color changes of pure DPPH solution with gradual addition of ascorbic acid; changes in absorbance of DPPH with complex addition; color changes of pure DPPH solution with gradual addition of complex; UV−vis spectra for the complex for day 1, 2, and 3; scatchard plots for DNA interaction of the complex in competitive experiments with EB and Hoechst at 298 K; Stern−Volmer plot and scatchard plot for BSA interaction of the complex at 298 K; bond distances (Å) and angles (°) for the complex $[Cu(L1)_2(L2)]^+(ClO_4)^-$; and nonclassic hydrogen bond dimensions for the complex $[Cu(L1)_2(L2)]^+(ClO_4)^-$ (PDF)

Molecular formula strings (CIF)

■ AUTHOR INFORMATION

Corresponding Authors

Sudipta Dalai − *Department of Chemistry and Chemical Technology, Vidyasagar University, Midnapore 721102 West Bengal, India*; Email: sudipta@mail.vidyasagar.ac.in

Keka Sarkar − *Department of Microbiology, University of Kalyani, West Bengal, Kalyani 741235, India*; Email: keka@klyuniv.ac.in

Bidhan Chandra Samanta − *Department of Chemistry, Mugberia Gangadhar Mahavidyalaya, 721425 Contai, West Bengal, India*; orcid.org/0000-0002-6029-371X; Email: bidhansamanta@yahoo.in, bsmgm1977@gmail.com

Authors

Arun Kuila − *Department of Chemistry, Mugberia Gangadhar Mahavidyalaya, 721425 Contai, West Bengal, India; Department of Chemistry and Chemical Technology, Vidyasagar University, Midnapore 721102 West Bengal, India*

Ribhu Maity − *Department of Chemistry, Mugberia Gangadhar Mahavidyalaya, 721425 Contai, West Bengal, India*

Prasun Acharya − *Department of Chemistry, Mugberia Gangadhar Mahavidyalaya, 721425 Contai, West Bengal, India; Department of Chemistry and Chemical Technology, Vidyasagar University, Midnapore 721102 West Bengal, India*

Tuhin Sarkar − *Department of Microbiology, University of Kalyani, West Bengal, Kalyani 741235, India*

Ankika Bhakat − *Department of Microbiology, University of Kalyani, West Bengal, Kalyani 741235, India*

Paula Brandao − *Departamento de Química, CICECO, Universidade de Aveiro, 3810-193 Aveiro, Portugal*

https://doi.org/10.1021/acsomega.4c05824
ACS Omega 2024, 9, 48273−48284

Satyajit Pattanayak − *Department of Chemistry, Mugberia Gangadhar Mahavidyalaya, 721425 Contai, West Bengal, India*

Tithi Maity − *Department of Chemistry, Prabhat Kumar College, 721401 Contai, West Bengal, India;* orcid.org/0000-0002-1256-399X

Complete contact information is available at: https://pubs.acs.org/10.1021/acsomega.4c05824

Notes

The authors declare no competing financial interest.

■ ACKNOWLEDGMENTS

B.C.S. expresses gratitude for the financial support from the Department of Biotechnology (DBT), Government of India, granted to Mugberia Gangadhar Mahavidyalaya under the Star College Strengthening Scheme (order no. HRD-11011/161/2020-HRD-DBT, dated 24/08/2020). P.B. expresses gratitude for the financial assistance received from national funds through the Foundation for Science and Technology (FCT) and the Ministry of Science, Technology, and Higher Education (MCTES) (Project CICECO-Aveiro Institute of Materials, UIDB/50011/2020, UIDP/50011/2020 & LA/P/0006/2020). A.K., P.A., and Ribhu Maity extend their appreciation to the authorities of Mugberia Gangadhar Mahavidyalaya for providing laboratory facilities essential for conducting the experiments.

■ REFERENCES

(1) Agwara, M. O.; Ndifon, P. I.; Ndosiri, N. B.; Paboudam, A. G.; Yufanyi, D. M.; Mohamadou, A. Synthesis, characterisation and antimicrobial activities of cobalt(II), copper(II) and zinc(II) mixed-ligand complexes containing 1,10-phenanthroline and 2,2'-bipyridine. *Bull. Chem. Soc. Ethiop.* **2010**, *24*, 383−389.

(2) Scozzafava, A.; Supuran, C. T. Carbonic anhydrase and matrix metalloproteinase inhibitors: Sulfonylated amino acid hydroxamates with MMP inhibitory properties act as efficient inhibitors of CA isozymes I, II, and IV, and N-hydroxysulfonamides inhibit both these zinc enzymes. *J. Med. Chem.* **2000**, *43*, 3677−3687.

(3) Easmon, J.; Pürstinger, G.; Heinisch, G.; Roth, T.; Fiebig, H. H.; Holzer, W.; Jäger, W.; Jenny, M.; Hofmann, J. Synthesis, Cytotoxicity, and Antitumor Activity of Copper(II) and Iron(II) Complexes of 4 N -Azabicyclo[3.2.2]Nonane Thiosemicarbazones Derived from Acyl Diazines. *J. Med. Chem.* **2001**, *44*, 2164−2171.

(4) Liang, F.; Wu, C.; Lin, H.; Li, T.; Gao, D.; Li, Z.; Wei, J.; Zheng, C.; Sun, M. Copper Complex of Hydroxyl-Substituted Triazamacrocyclic Ligand and Its Antitumor Activity. *Bioorg. Med. Chem. Lett.* **2003**, *13*, 2469−2472.

(5) Dharmaraj, N.; Viswanathamurthi, P.; Natarajan, K. Ru(II) complexes containing bidendate Schiff bases and their antifungal activity. *Transition Met. Chem.* **2001**, *26*, 105−109.

(6) Chaudhary, A.; Bansal, N.; Gajraj, A.; Singh, R. V. Antifertility, antibacterial, antifungal and percent disease incidence aspects of macrocyclic complexes of Mn(II). *J. Inorg. Biochem.* **2003**, *96*, 393−400.

(7) Balan, A. M. K. R.; Ashok, R. F. N.; Vasanthi, M.; Prabu, R.; Paulraj, A. Mixed ligand complexes of nickel(II), copper(II) and zinc(II) with nicotinanilide and thiocyanate. *Int. J. Life Sci. Pharm. Rev.* **2013**, *3*, 67−75.

(8) Rajalakshmi, S.; Kiran, M. S.; Nair, B. U. DNA condensation by copper(II) complexes and their anti-proliferative effect on cancerous and normal fibroblast cells. *Eur. J. Med. Chem.* **2014**, *80*, 393−406.

(9) Arjmand, F.; Sharma, G. C.; Muddassir, M.; Tabassum, S. Synthesis and enantiopreferential DNA-binding profile of late 3d transition metal R- and S-enantiomeric complexes derived from N,N-bis-(1-benzyl-2-ethoxyethane): validation of R-enantiomer of copper-(II) complex as a human topoisomerase II inhibitor. *Chirality* **2011**, *23*, 557−567.

(10) Komor, A. C.; Barton, J. K. The path for metal complexes to a DNA target. *Chem. Commun.* **2013**, *49*, 3617−3630.

(11) Pravin, N.; Raman, N. Investigation of in vitro anticancer and DNA strap interactions in live cells using carboplatin type Cu(II) and Zn(II) metalloinsertors. *Eur. J. Med. Chem.* **2014**, *85*, 675−687.

(12) Santini, C.; Pellei, M.; Gandin, V.; Porchia, M.; Tisato, F.; Marzano, C. Advances in Copper Complexes as Anticancer Agents. *Chem. Rev.* **2014**, *114*, 815−862.

(13) Kumar, M.; Kumar, G.; Dadure, K. M.; Masram, D. T. Copper(II) complexes based on levofloxacin and 2N-donor ligands: synthesis, crystal structures and in vitro biological evaluation. *New J. Chem.* **2019**, *43*, 15462−15481.

(14) Kumar, M.; Kumar, G.; Masram, D. T. Copper(II) complexes containing enoxacin and heterocyclic ligands: synthesis, crystal structures and their biological perspectives. *New J. Chem.* **2020**, *44*, 8595−8613.

(15) Krishnamoorthy, P.; Sathyadevi, P.; Cowley, A. H.; Butorac, R. R.; Dharmaraj, N. Evaluation of DNA Binding, DNA Cleavage, Protein Binding and in Vitro Cytotoxic Activities of Bivalent Transition Metal Hydrazone Complexes. *Eur. J. Med. Chem.* **2011**, *46*, 3376−3387.

(16) Ma, Y.; Cao, L.; Kawabata, T.; Yoshino, T.; Yang, B. B.; Okada, S. Cupric Nitrilotriacetate Induces Oxidative DNA Damage and Apoptosis in Human Leukemia HL-60 Cells. *Free Radical Biol. Med.* **1998**, *25*, 568−575.

(17) Arjmand, F.; Jamsheera, A.; Mohapatra, D. K. Synthesis, Characterization and in Vitro DNA Binding and Cleavage Studies of Cu(II)/Zn(II) Dipeptide Complexes. *J. Photochem. Photobiol., B* **2013**, *121*, 75−85.

(18) Zhou, N.; Liang, Y. Z.; Wang, P. 18β-Glycyrrhetinic acid interaction with bovine serum albumin. *J. Photochem. Photobiol., A* **2007**, *185*, 271−276.

(19) Shang, L.; Jiang, X.; Dong, S. In vitro study on the binding of neutral red to bovine serum albumin by molecular spectroscopy. *J. Photochem. Photobiol., A* **2006**, *184*, 93−97.

(20) Singh, S.; Singh, R. P. In vitro methods of assay of antioxidants: An overview. *Food Rev. Int.* **2008**, *24*, 392−415.

(21) Cui, K.; Luo, X.; Murthy, M. R. V. Role of oxidative stress in neurodegeneration: recent developments in assay methods for oxidative stress and nutraceutical antioxidants. *Prog. Neuropsychopharmacol. Biol. Psychiatry* **2004**, *28*, 771−799.

(22) Kedare, S. B.; Singh, R. P. Genesis and development of DPPH method of antioxidant assay. *J. Food Sci. Technol.* **2011**, *48*, 412−422.

(23) Nganje, W. E.; Bangsund, D. A.; Leistritz, F. L.; Wilson, W. W.; Tiapo, N. M. Regional Economic Impacts of Fusarium Head Blight in Wheat and Barley. *Appl. Econ. Perspect. Policy* **2004**, *26*, 332−347.

(24) Jones, J. P.; Jones, J.; Miller, J. *Fusarium wilt of tomato*; Florida Department of Agriculture and Consumer Services, 1982.

(25) Tiwari, N.; Ahmed, S.; Kumar, S.; Sarker, A. Fusarium wilt: a killer disease of lentil. In *Fusarium: Plant Diseases, Pathogen Diversity, Genetic Diversity, Resistance and Molecular Markers*; Askun, T., Ed.; Books on Demand, 2018.

(26) Gawehns, F.; Ma, L.; Bruning, O.; Houterman, P. M.; Boeren, S.; Cornelissen, B. J. C.; Rep, M.; Takken, F. L. W. The effector repertoire of Fusarium oxysporum determines the tomato xylem proteome composition following infection. *Front. Plant Sci.* **2015**, *6*, 967.

(27) Saha, M.; Mandal, S.; Bhakat, A.; Sarkar, K.; Chattopadhyay, A. P.; Saha, N. C. Synthesis, characterization, photoluminescence properties, DFT studies, photocatalytic and antifungal activity of a new pyrazole-containing thiosemicarbazone ligand and its Co (III) and Ni (II) complexes. *J. Coord. Chem.* **2023**, *76* (9−10), 1261−1280.

(28) Mandal, S.; Bhakat, A.; Banerjee, S.; Sarkar, K.; Cordes, D. B.; Slawin, A. M.; Saha, N. C. Antifungal and antibacterial activity of two new Ni (II) complexes of a pyrazole-appended thiophene containing bidentate schiff-base ligand: Synthesis, spectroscopy and crystal structures. *J. Mol. Struct.* **2024**, *1313*, 138688.

(29) Sheldrick, G. M. A short history of SHELX. *Acta Crystallogr., Sect. A: Found. Crystallogr.* **2008**, *64*, 112−122.
(30) MacRae, C. F.; Sovago, I.; Cottrell, S. J.; Galek, P. T. A.; McCabe, P.; Pidcock, E.; Platings, M.; Shields, G. P.; Stevens, J. S.; Towler, M.; Wood, P. A. Mercury 4.0: From Visualization to Analysis, Design and Prediction. *J. Appl. Crystallogr.* **2020**, *53*, 226−235.
(31) CCDC Cambridge database ConQuest version 2022.3.0.
(32) Jagadeesan, S.; Balasubramanian, V.; Baumann, P.; Neuburger, M.; Häussinger, D.; Palivan, C. G. Water soluble Co(III) complexes of substituted phenanthrolines with cell selective anticancer activity. *Inorg. Chem.* **2013**, *52*, 12535−12544.
(33) Blois, M. S. Antioxidant determinations by the use of a stable free radical. *Nature* **1958**, *181*, 1199−1200.
(34) Bhakat, A.; Sen, S.; Banerjee, S.; Sarkar, K. Plant growth promotion and lipopeptide-mediated biological control of chilli pathogen Colletotrichum siamense by endophytic Bacillus sp. *Physiol. Mol. Plant Pathol.* **2023**, *125*, 102026.
(35) Butt, S. S.; Badshah, Y.; Shabbir, M.; Rafiq, M. Molecular Docking Using Chimera and Autodock Vina Software for Non-bioinformaticians. *JMIR Bioinform. Biotechnol.* **2020**, *1*, No. e14232.
(36) Taghizadeh, M. S.; Niazi, A.; Moghadam, A.; Afsharifar, A. Experimental, molecular docking and molecular dynamic studies of natural products targeting overexpressed receptors in breast cancer. *PLoS One* **2022**, *17*, No. e0267961.
(37) Maity, M.; Maity, R.; Sarkar, T.; Bhakat, A.; Brandao, P.; Maity, T.; Das, P.; Sarkar, K.; Samanta, B. C. In Vitro Insight on Antifungal-Specific Potentiality of Ni(II) Complex against Colletotrichum siamense and Fusarium equisetum Phytopathogens. *ACS Appl. Bio Mater.* **2023**, *6*, 4836−4845.
(38) Yilmaz, V. T.; Icsel, C.; Turgut, O. R.; Aygun, M.; Erkisa, M.; Turkdemir, M. H.; Ulukaya, E. Synthesis, structures and anticancer potentials of platinum (II) saccharinate complexes of tertiary phosphines with phenyl and cyclohexyl groups targeting mitochondria and DNA. *Eur. J. Med. Chem.* **2018**, *155*, 609−622.
(39) Tian, N.; Zhou, Z. Y.; Sun, S. G.; Ding, Y.; Wang, Z. L. Synthesis of tetrahexahedral platinum nanocrystals with high-index facets and high electro-oxidation activity. *Science* **2007**, *316*, 732−735.
(40) Acharya, P.; Maity, R.; Kuila, A.; Maity, T.; Maity, S.; Sepay, N.; Samanta, B. C. Hydrophobicity-induced DNA, BSA binding, and biomaterial applications of a heteroleptic Cu (II) complex. *Appl. Organomet. Chem.* **2022**, *36*, No. e6640.
(41) Maity, R.; Maity, M.; Jana, K.; Maity, T.; Sepay, N.; Samanta, B. C. Unveiling the catecholase activities and DNA binding interaction of mono-di-and polymeric Cu(II) complexes derived from heterogeneous Schiff base ligands. *New J. Chem.* **2023**, *47*, 2673−2681.
(42) Maity, R.; Manna, B.; Maity, S.; Jana, K.; Maity, T.; Afzal, M.; Sepay, N.; Samanta, B. C. Synthesis of an Aryl-Semicarbazone-Based Cu(II) Complex for DNA and BSA Interaction and Anti-Cancer Activity against Human Cervix Uteri Carcinoma. *Inorganics* **2024**, *12*, 19.
(43) Lian, W.-J.; Wang, X.-T.; Xie, C.-Z.; Tian, H.; Song, X.-Q.; Pan, H.-T.; Qiao, X.; Xu, J.-Y. Mixed-ligand copper(II) Schiff base complexes: the role of the co-ligand in DNA binding, DNA cleavage, protein binding and cytotoxicity. *Dalton Trans.* **2016**, *45*, 9073−9087.
(44) Acharya, P.; Kuila, A.; Pramanik, U.; Hathwar, V. R.; Brandao, P.; Mukherjee, S.; Maity, S.; Maity, T.; Maity, R.; Samanta, B. C. Combined theoretical and experimental insights on DNA and BSA binding interactions of Cu(II) and Ni(II) complexes along with the DPPH method of antioxidant assay and cytotoxicity studies. *RSC Adv.* **2023**, *13*, 7632−7644.
(45) Mitra, A.; Saikh, F.; Das, J.; Ghosh, S.; Ghosh, R. Studies on the interaction of a synthetic nitro-flavone derivative with DNA: A multi-spectroscopic and molecular docking approach. *Spectrochim. Acta, Part A* **2018**, *203*, 357−369.

https://doi.org/10.1021/acsomega.4c05824
ACS Omega 2024, 9, 48273−48284